

Electrical dark compacton generator: Theory and simulationsFabien Kenmogne,^{1,*} David Yemélé,^{2,†} and Paul Wofo^{1,‡}¹*Laboratory of Modelling and Simulation in Engineering and Biological Physics, Faculty of Science, University of Yaoundé I, P. O. Box 812, Yaoundé, Cameroon*²*Laboratoire de Mécanique et de Modélisation des Systèmes Physiques L2MSP, Faculté des Sciences, Université de Dschang, Boîte Postale 067, Dschang, Cameroon*

(Received 16 October 2011; revised manuscript received 6 March 2012; published 22 May 2012)

A modified Colpitts oscillator (MCO) associated with a nonlinear transmission line (NLTL) with intersite nonlinearity is introduced as a self-sustained generator of a train of modulated dark signals with compact shape. Equations of state describing the dynamics of the MCO part are derived and the stationary state is obtained. Using the Routh-Hurwitz criterion, the result of a stability analysis indicates the existence of a limit cycle in certain parameter regimes and there the oscillation of the circuit delivers pulselike electrical signals. The train of generated signals is then transformed into a train of compact modulated dark voltage solitons by the NLTL. The exactness of this analytical analysis is confirmed by numerical simulations performed on the circuit equations. Finally, simulations show the capacity of this circuit to work as a generator of compactlike dark voltage solitons. The performance of the generator, namely, the pulse width and the repetition rate, is controlled by the magnitude of the characteristic parameters of the electronic components of the device.

DOI: [10.1103/PhysRevE.85.056606](https://doi.org/10.1103/PhysRevE.85.056606)

PACS number(s): 05.45.Yv, 84.30.Ng, 07.50.Qx

I. INTRODUCTION

In electronics, as first demonstrated by Hirota and Suzuki [1], a nonlinear electrical transmission line (NLTL) serves as a nonlinear dispersive medium that propagates nonlinear localized excitations or solitons. Since this pioneering work, there has been increasing interest in the use of NLTLs for studying nonlinear phenomena in general and bright and dark solitons in particular [2]. Numerical simulations show that dark solitons are more stable than bright solitons in the presence of noise and spread more slowly in the presence of system loss. They are also less affected by many other factors that have an impact on the use of bright solitons. These properties point to potential applications of dark solitons for communication systems [3,4].

In recent years the development in NLTLs has demonstrated their capacity to work as signal processing tools. To cite only a very few examples, it has been demonstrated that a nonlinear uniform electrical line can be used for extremely wideband signal shaping applications [5] and also as a waveform equalizer in a compensation scheme for signal distortion caused by optical fiber polarization dispersion modes [6]. Moreover, it is also possible to use NLTLs for controlling the amplitude (amplification) [7,8] and the delay of ultrashort pulses through the coupled propagation of the solitonic and dispersive parts, which is important in that it enables the characterization of high-speed electronic devices such as heterojunction field effect transistors or resonant tunneling diodes, and raises the possibility of establishing future ultrahigh-speed signal processing technologies [9]. In modern electronics such as ultrafast time-domain metrology, short-duration electrical solitons play an important role since they are used to sample rapidly varying signals or as probe signals in ranging radar and time-domain reflectometry [10,11]. Similarly, it is also possible to use these short-duration pulses as carrier signals in communication [12].

It is then of great interest to look for electronic devices capable of generating these pulse solitons. In this context, NLTLs have also been used as two-port devices to produce pulse solitons. *This two-port topology of the NLTL requires an external high-frequency input, and the output waveform is sensitive to the quality and shape of the input signal.* An extension was the construction of a one-port electrical circuit that self-generates a periodic and stable train of electrical bright solitons with no high-frequency input, through a combination of a NLTL with a special amplifier in a circular topology [13].

In this paper, we introduce an intermediate extension between one-port and two-port electrical circuits, consisting of a two-port electrical circuit that includes the advantages of a one-port circuit. This generator is a combination of a modified Colpitts oscillator and a special NLTL [14] capable of propagating a compact signal. It self-starts by growing from ambient noise to produce a harmonic electrical signal, which is transformed into a train of compact electrical pulses, going through the NLTL, and thus making a self-sustained dark compacton generator that does not require an external high-frequency input. Unlike soliton signals, compacton signals are ultralocalized and do not interact with each other. In fact, over a decade ago, Rosenau and Hyman [15] studied a special type of nonlinear partial differential equation, a Korteweg–de Vries equation with nonlinear dispersion and introduced a class of solitary waves with compact support, outside of which they vanish identically. The solutions were found to emerge unaltered from collisions and were thus called compactons [15], analogous to solitons since they retain their identity after multiple collisions. Because of their compact structure, neither compactons nor antcompactons interact with each other until the moment of collision. In other words, *two adjacent compactons do not interact unless they come into contact in a way similar to the contact between hard spheres.* Because of the compacton's finite extension, its experimental realization is possible only with a finite background instead of the infinite background associated with gray solitons. In addition, numerical calculations show that gray solitons with a

*kenfabien@yahoo.fr

†dyemele@yahoo.fr

‡pwoafo1@yahoo.fr

finite background pulse exhibit propagation properties nearly identical to those of solitons with infinite background only if the background pulse is wider by a factor of 10 or more than the soliton [16]. Thus, the use of gray compactons which are strictly localized (finite extension) will allow these difficulties to be overcome and will also increase substantially the data repetition rate when they are invoked to codify data. Similarly, since the gray compacton width is also independent of the amplitude, in contrast to the gray soliton width which is amplitude dependent, gray-compacton-like signals with arbitrary amplitude cannot disintegrate into other compactons during propagation and consequently should be more stable in the network compared to the classical gray solitons.

The paper is organized as follows. We first present the topology of the dark compacton generator in Sec. II. Next, in Sec. III, the equations governing the dynamics of the oscillator are derived and used to study analytically the behavior of the circuit. In Sec. IV, numerical simulations as well as experiments by means of the PSPICE professional simulator are performed. Finally, Sec. V is devoted to discussion and concluding remarks.

II. NLTL DARK COMPACTON GENERATOR TOPOLOGY

In this section, we describe the physical structure of the compact dark generator as depicted in Fig. 1. This generator

consists of a coupling between a modified Colpitts oscillator (MCO) and a nonlinear electrical transmission line with nonlinear dispersion.

A. Modified Colpitts oscillator

Because of the richness of its dynamical behavior and also its ability to produce chaotic signals, the Colpitts oscillator is used in a variety of applications including signal masking [17], chaos modulation [18,19], and spectrum spreading [20]. In fact the basic Colpitts oscillator is a combination of a transistor amplifier and LC circuits used to feed back the output signal [21,22]. It is easily realizable, easily modeled, and scalable in frequency. Its frequency of operation can vary from a few hertz up to gigahertz, depending on the technology, and thus it is frequently used for practical and commercial technology [22]. In this paper, it is used as a part of a more complex oscillator, named the MCO, which consists of four different blocks as follows (see Fig. 1):

The first block is the basic Colpitts oscillator with the transistor Q used in the common-base configuration and modeled by the linear current controlled source $I_C = \alpha_F I_E$, where $\alpha_F = \beta_F / (1 + \beta_F)$ is the common-base forward current gain ($0 < \alpha_F < 1$) and β_F the common-emitter forward current gain. I_C and I_E are the base-collector and base-emitter currents, respectively. The intrinsic nonlinearity of the system

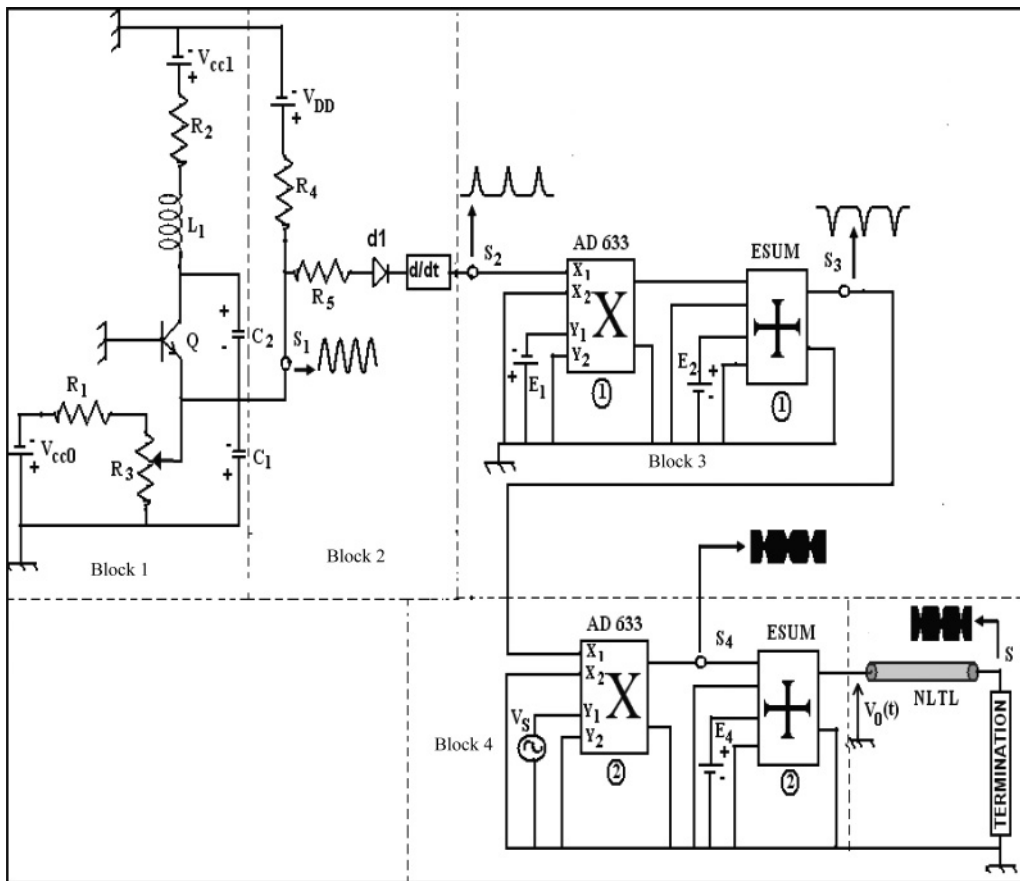


FIG. 1. Schematic diagram of a self-sustained dark compacton generator. The generator is constituted of the NLTL bloc and four other blocks: the classical Colpitts oscillator, an adapter of compact pulse signals, an inverter and the modulation circuit. The NLTL bloc contains the NLTL ended by the termination which prevents reflexions by absorbing signal voltage that can reflect at the end of the line.

is described by [23]

$$I_C = I_s[\exp(V_{BE}/V_T) - 1], \quad (1)$$

where I_s is the saturation current of the base-emitter junction and $V_T = 26$ mV the thermal voltage at room temperature.

The second block is the compact pulse signal adapter containing among many electronic components an ideal diode d_1 with the input-output voltage characteristic given by

$$V_{\text{out}} = \begin{cases} G(V_{\text{in}} - V_{th}) & \text{if } V_{\text{in}} > V_{th}, \\ 0 & \text{otherwise,} \end{cases} \quad (2)$$

where G is the voltage gain of the diode and V_{th} the threshold value of the voltage. The third block is constituted of a voltage electronic summer ESUM(1) and a voltage four-quadrant analog multiplier AD633 (1) with the input-output relationship given by

$$W = \Gamma(X_2 - X_1)(Y_2 - Y_1), \quad (3)$$

where X_1 , X_2 , Y_1 , and Y_2 are the input voltages of the multiplier, and $\Gamma = 0.1 \text{ V}^{-1}$ is the modulation coefficient. Finally, the last block is the modulation circuit. The fundamental frequency of the MCO can be estimated as [23]

$$f^* = \omega_{\text{ref}}/2\pi, \quad \omega_{\text{ref}} = \left(L_1 \frac{C_1 C_2}{C_1 + C_2} \right)^{-1/2}, \quad (4)$$

so that its variation can be achieved by varying the capacitance C_1 and/or C_2 .

As a basic Colpitts oscillator, the MCO described above may behave as a self-sustained oscillator capable of generating chaotic and regular signals. More interestingly, it is especially designed to produce, under certain conditions, a well-defined type of regular signal, namely, a *pulse train of signal voltages* with high frequency. This particular signal voltage is indispensable for the NLTL part to generate a train of compact modulated dark solitary waves when the two parts of the circuits are dynamically *synchronized* (synchronization here and hereafter means that signals generated by the MCO part and by the NLTL part have the same shape). Similarly, the considered NLTL has to be built conveniently to exhibit compact waves instead of standard solitons, as described below.

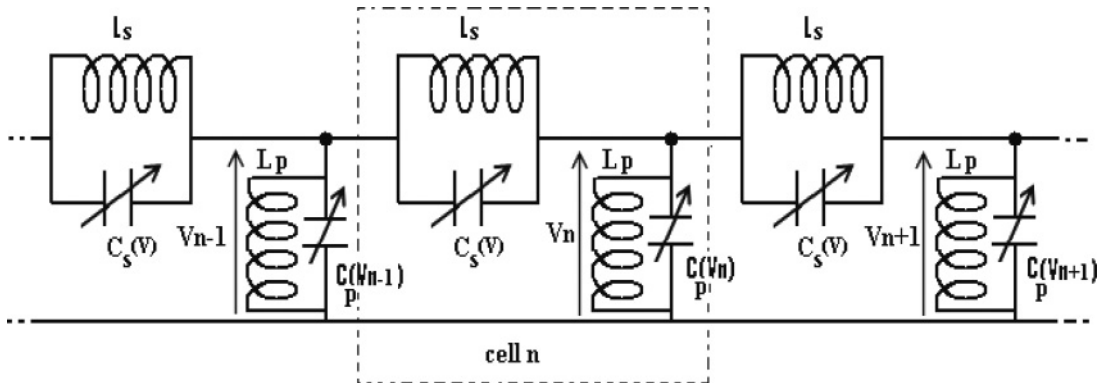


FIG. 2. Schematic representation of the nonlinear transmission line. Each cell contains, in the series branch, a linear inductor L_s shunted by a nonlinear capacitor $C_s(V)$, and in the shunted branch, a nonlinear capacitor $C_p(V_n)$ shunted by another linear inductor L_p .

B. NLTL description

The NLTL part is an LC ladder. The equivalent circuit is shown in Fig. 2, in which the unit cell contains both a series linear inductor L_s shunted by a capacitor $C_s(V)$ while L_p and $C_p(V)$ represent the shunt inductor and capacitor, respectively. The two capacitors are varactors (e.g., reverse-biased p - n junction diodes or metal-oxide-semiconductor capacitors). The nonlinearity of the NLTL results from the varactors, whose capacitance changes with applied voltage, while its dispersion arises from the linear inductor. The capacitance-voltage relationship is assumed to be Taylor expanded to second order and reads [24]

$$C_p(V_n + V_b) = C_{0p}(1 - 2\alpha V_n + 3\beta V_n^2) \quad (5)$$

for the shunt capacitor and

$$C_s(\delta V) = C_{0s}(1 - 2\eta\delta V + 3\lambda\delta V^2) \quad (6)$$

for the series capacitors, where C_{0s} is the capacitance at the zero-bias voltage while C_{0p} is the capacitance at the bias voltage V_b of the shunt capacitor. V_n is the voltage at node n while δV_n is the voltage across the series capacitor. This series capacitor induces nonlinear dispersion in the NLTL and is responsible for the compactification of the envelope of dark solitary waves [14].

III. NLTL COMPACTON GENERATOR: EQUATIONS OF STATE AND DYNAMICS

A. Transmission equation reconsidered

By applying Kirchhoff's laws to the n th cell of the circuit in Fig. 2, one obtains the transmission equation of the NLTL given by [14]

$$\begin{aligned} & \frac{d^2 V_n}{dt^2} + u_0^2(2V_n - V_{n-1} - V_{n+1}) + \omega_0^2 V_n \\ & - \alpha \frac{d^2 V_n^2}{dt^2} + \beta \frac{d^2 V_n^3}{dt^2} \\ & = C_{0r} \frac{d^2}{dt^2} \{ (V_{n-1} + V_{n+1} - 2V_n) \\ & - \eta[(V_{n-1} - V_n)^2 - (V_n - V_{n+1})^2] \\ & + \lambda[(V_{n-1} - V_n)^3 - (V_n - V_{n+1})^3] \} \end{aligned} \quad (7)$$

for $n = 1, 2, \dots, N - 1$, and with

$$C_{0r} = C_{0s}/C_{0p}, \quad \omega_0^2 = 1/L_p C_{0p}, \quad u_0^2 = 1/L_s C_{0p}. \quad (8)$$

The constant C_{0r} is the dimensionless capacitance while u_0 and ω_0 are the characteristic frequencies of the system. The linear frequency ω and wave number k of the linear wave (a wave with small amplitude) satisfy the linear dispersion law

$$\omega^2 = \frac{\omega_0^2 + 4u_0^2 \sin^2(k/2)}{1 + 4C_{0r} \sin^2(k/2)}, \quad (9)$$

which describes the bandpass-filter character of the network in this regime, with the gap frequency ω_0 and the cutoff frequency

$$\omega_c^2 = (\omega_0^2 + 4u_0^2)/(1 + 4C_{0r}). \quad (10)$$

As demonstrated by Yemélé and Kenmogné [14], in the nonlinear regime and when the electrical pulse width is much greater than the lattice spacing, the dynamics of the amplitude $A(x, t)$ of modulated nonlinear waves of the form

$$V_n(t) = A(x, t) \exp[i(kn - \omega t)] + \text{c.c.} \quad (11)$$

satisfies the following extended nonlinear Schrödinger equation (ENLS) equation

$$i \frac{\partial A}{\partial \tau} + P \frac{\partial^2 A}{\partial X^2} + Q |A|^2 = ir_1 \frac{\partial A}{\partial X} |A|^2 + r_{23} A^* \frac{\partial^2 A^2}{\partial X^2} + r_3 A \frac{\partial^2 (|A|^2)}{\partial X^2}, \quad (12)$$

where the coefficients P , Q , r_1 , r_{23} , and r_3 depends both on the characteristic parameters of the network and on the parameters of the input carrier waves:

$$P = -\frac{1}{2\omega} \frac{(v_g/\omega)(u_0^2 + 3C_{0r}\omega^2) \sin k + (C_{0r}\omega^2 - u_0^2) \cos k}{1 + 4C_{0r} \sin^2(k/2)},$$

$$Q = \frac{3\omega \beta - 16C_{0r}\lambda \sin^4(k/2)}{2(1 + 4C_{0r} \sin^2(k/2))},$$

$$V_n(t) = \begin{cases} V_m \sin \mu_c(n - n_0 - v_c t) \cos[(kn - \omega t)], & |(n - n_0 - v_c t)| \leq \pi/2\mu_c, \\ V_m \cos[(kn - \omega t)], & (n - n_0 - v_c t) > \pi/2\mu_c, \\ -V_m \cos[(kn - \omega t)], & (n - n_0 - v_c t) < -\pi/2\mu_c, \end{cases} \quad (19)$$

where μ_c is the width parameter and v_c the velocity of the signal in the network. Their expressions are

$$\mu_c = \left[\frac{r_1^2 - 16r_{23}Q}{64r_{23}(r_{23} + r_3)} \right]^{1/2} \quad \text{and} \quad v_c = v_g - \frac{Pr_1}{4r_3}. \quad (20)$$

Unlike standard dark solitons with infinite extension, the solution (19) is strictly localized in the region of space $\pi/2\mu_c$ and defines the analytical expression of the dark-compacton-like signal voltages exhibited by the NLTL. Note that the signal in the region $|n - n_0 - v_c t| > \pi/2\mu_c$ defines the background intensity and has an arbitrary extension, leading to the possibility of obtaining a train of dark solitary

$$r_1 = 24C_{0r}\lambda\omega \frac{\sin k \sin^2(k/2)}{1 + 4C_{0r} \sin^2(k/2)},$$

$$r_{23} = 2C_{0r}\lambda\omega \frac{\sin(k/2) \sin(3k/2)}{1 + 4C_{0r} \sin^2(k/2)},$$

and

$$r_3 = -6C_{0r}\lambda\omega \frac{\sin^2(k/2)}{1 + 4C_{0r} \sin^2(k/2)}. \quad (13)$$

The variables X and τ are related to the cell number n and time t as follows:

$$X = n - v_g t \quad \text{and} \quad \tau = t, \quad (14)$$

where

$$v_g \equiv \frac{d\omega}{dk} = \frac{1}{\omega} \frac{(u_0^2 - C_{0r}\omega^2) \sin k}{1 + 4C_{0r} \sin^2(k/2)} \quad (15)$$

represents the group velocity of the wave-packet. This ENLS equation admits a compact dark solution with the form

$$A(X, \tau) = A_0 \sin \mu(X - X_0 - v_e \tau) \exp[i\gamma(X - v_p \tau)],$$

$$|(X - X_0 - v_e \tau)| \leq \pi/2\mu, \quad (16)$$

with

$$\gamma = \frac{-r_1}{8r_{23}}, \quad v_e = 2P\gamma, \quad (17)$$

and

$$v_p = \gamma P - \left(\frac{P}{2(r_3 + r_{23})} + A_0^2 \right) \left(\frac{r_1}{4} + \frac{Q}{2\gamma} \right). \quad (18)$$

Going back to the original variables, that is the cell number n and time t , it is then easy to show that the circuit equation (7) has the following compact solution:

waves with arbitrary period ℓ provided that $\ell > \pi/2\mu_c$. The envelope part of this signal is depicted in Fig. 3.

B. MCO dynamics

1. State equations: Steady state solution and stability

Denoting by V_{c1} and V_{c2} the voltages across the capacitors C_1 and C_2 of the MCO, respectively, and applying Kirchhoff's laws to the circuit of Fig. 1, we obtain the following set of ordinary differential equations governing the dynamics of the system:

$$\begin{cases} C_1 \frac{dV_{c1}}{dt} = \frac{V_{cc0}}{R_1 + \alpha R_3} - \frac{V_{DD}}{R_4} - \frac{V_{c1}}{R_{EE}} - I_L - \frac{I_C}{\beta_F}, \\ C_2 \frac{dV_{c2}}{dt} = I_L - I_C, \\ L_1 \frac{dI_L}{dt} = V_{cc1} + V_{c1} - V_{c2} - R_2 I_L, \end{cases} \quad (21)$$

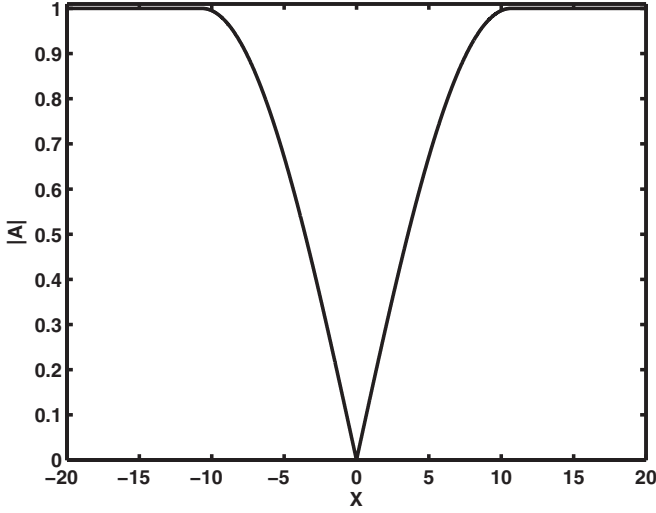


FIG. 3. Single compact dark solitary wave profile (envelope part) located at $X_0 = 0$ with amplitude $A_0 = 1$ and width $\mu = 0.1472$.

with

$$R_{EE} = \left[\frac{R_1 + R_3}{(1 - \chi)R_3(R_1 + \chi R_3)} + \frac{1}{R_4} + \frac{1}{R_5} \right]^{-1}, \quad (22)$$

where the parasitic effects in the base-emitter capacitor C_{be} and collector-emitter capacitor C_{ce} are neglected. In these equations, χ is the shunt coefficient of the emitter resistor R_3 where V_{c1} , V_{c2} , and I_L are the circuit-state variables, while I_C is defined by Eq. (1). Here, $V_{BE} = V_{c1}$ and the output signal at gate S_1 is $V_{S1} = V_{c1}$ while at gates S_2 and S_3 the output signals obtained according to Eqs. (2) and (3) are

$$V_{S2} = G \frac{dV_{c1}}{dt} \quad \text{and} \quad V_{S3} = -G\Gamma E_1 \frac{dV_{c1}}{dt} + E_2 \quad (23)$$

for $dV_{c1}/dt > 0$; $V_{S2} = 0$ and $V_{S3} = E_2$, otherwise. E_1 and E_2 are dc voltages, with $E_2 \geq G\Gamma E_1 |dV_{c1}/dt|$. It appears from Eqs. (21) and (23) that the dynamics of the MCO is similar to that of a master-slave system in which the first block behaves as the master while the second and the third blocks are the slaves. If the current I_c is neglected in Eq. (21), the MCO admits a single equilibrium or steady state solution $(\overline{V_{c1}}, \overline{V_{c2}}, \text{ and } \overline{I_L})$, obtained by setting the right-hand side of Eq. (21) to zero:

$$\begin{aligned} \overline{V_{c1}} &= \frac{R_{EE} V_{cc0}}{R_1 + \alpha R_3} - \frac{R_{EE} V_{DD}}{R_4}, \\ \overline{V_{c2}} &= V_{c1} + \frac{R_{EE} V_{cc0}}{R_1 + \alpha R_3} - \frac{R_{EE} V_{DD}}{R_4}, \\ \overline{I_L} &= 0. \end{aligned} \quad (24)$$

where R_{EE} is the equivalent emitter resistance, V_{CC} and V_{DD} are the direct current supplied voltages, and R_1, R_2, R_4 and R_5 are the resistances. By rescaling V_{c1} , V_{c2} , I_L , and the time t , Eq. (21) may then be rewritten in the following dimensionless form:

$$\frac{dX}{d\tau} = F(X), \quad (25)$$

where $X = (x_1, x_2, x_3)^T$, with

$$x_1 = \frac{(V_{c1} - \overline{V_{c1}})}{V_T}, \quad x_2 = \frac{(V_{c2} - \overline{V_{c2}})}{V_T}, \quad x_3 = \frac{R(I_L - \overline{I_L})}{V_T}, \quad (26)$$

and $\tau = \omega_{\text{ref}} t$, where ω_{ref} is the fundamental frequency defined in Eq. (4). Similarly, the vector field $F = (f_1, f_2, f_3)^T$ is given by

$$\begin{aligned} f_1 &= -a_1[\gamma_1 x_1 + x_3 + \rho g(x_1)/\beta_F], \\ f_2 &= \epsilon a_1 [x_3 - \rho g(x_1)], \\ f_3 &= a_3(x_1 - x_2 - x_3). \end{aligned} \quad (27)$$

The dimensionless parameters ϵ , a_1 , a_3 , γ_1 , and ρ are given by

$$\begin{aligned} \epsilon &= C_1/C_2, \quad a_1 = \frac{1}{C_1 R_2 \omega_{\text{ref}}}, \quad a_3 = \frac{R_2}{L_1 \omega_{\text{ref}}}, \\ \gamma_1 &= R_2/R_{EE}, \end{aligned}$$

and

$$\rho = \frac{R_2 I_S}{V_T} \exp \left[\frac{R_{EE}}{V_T} \left(\frac{V_{cc0}}{R_1 + \chi R_3} - \frac{V_{DD}}{R_4} \right) \right], \quad (28)$$

while the nonlinear function $g(x_1)$ is defined as

$$g(x_1) = \exp(x_1) - g_0, \quad g_0 = \frac{R_2 I_S}{\rho V_T}. \quad (29)$$

Accordingly, and from Eq. (23), the dimensionless output voltages V_{S1} , V_{S2} , and V_{S3} are $x_{S1} = x_1$ and

$$x_{S2} = G \frac{dx_1}{d\tau} \quad \text{and} \quad x_{S3} = -G\Gamma E_1 \frac{dx_1}{d\tau} + E_2/V_T \quad (30)$$

if $dx_1/d\tau > 0$, and $x_{S2} = 0$ and $x_{S3} = E_2/V_T$, otherwise, with $x_{S2} = V_{S2}/V_T$ and $x_{S3} = V_{S3}/V_T$. In addition to Eq. (30), the set of ordinary differential equations (25) governs the dynamics of the MCO.

Physically, a steady state solution corresponds to an equilibrium state of the system and the behavior of the system may depend on its stability. To test this stability, let us consider the state vector $X = X_0 + \delta X$, where δX is the perturbation of the equilibrium solution $X_0(x_{10}, x_{20}, x_{30})$ given by

$$x_{20} = (1 + \gamma_1 \alpha_F) x_{10}, \quad x_{30} = -\gamma_1 \alpha_F x_{10}. \quad (31)$$

The component x_{10} satisfies the following equation:

$$\gamma_1 x_{10} + \rho g(x_{10})/\alpha_F = 0, \quad (32)$$

which has the solution

$$x_{10} = \frac{\rho g_0}{\gamma_1 \alpha_F} - W \left[\frac{\rho}{\gamma_1 \alpha_F} \exp \left(\frac{\rho g_0}{\gamma_1 \alpha_F} \right) \right], \quad (33)$$

where W is the Lambert W function [23,25].

The stability of this equilibrium state X_0 against the perturbation δX depends on the properties of the eigenvalues of the Jacobian matrix $J(X_0)$ given by

$$J = \begin{pmatrix} -a_1[\gamma_1 + \rho \exp(x_{10})/\beta_F] & 0 & -a_1 \\ -\epsilon a_1 \rho \exp(x_{10}) & 0 & \epsilon a_1 \\ a_3 & -a_3 & -a_3 \end{pmatrix}, \quad (34)$$

where $J_{ij} = \partial f_i / \partial X_j$. In fact, the equilibrium solution X_0 is stable if all the eigenvalues of J have zero or negative real parts. These eigenvalues satisfy the following characteristic equation:

$$\begin{aligned} Z^3 &+ \{a_3 + a_1[\gamma_1 + \rho \exp(x_{10})/\beta_F]\} Z^2 \\ &+ a_3 a_1 [1 + \epsilon + \gamma_1 + \rho \exp(x_{10})/\beta_F] Z \\ &+ \epsilon a_3 a_1^2 [\gamma_1 + \rho \exp(x_{10})/\alpha_F] = 0. \end{aligned} \quad (35)$$

According to the Routh-Hurwitz criterion, all roots of Eq. (35) would have negative real parts if the following conditions are satisfied:

$$a_3 + a_1[\gamma_1 + \rho \exp(x_{10})/\beta_F] > 0 \quad (36)$$

and

$$\begin{aligned} & \{a_3 + a_1[\gamma_1 + \rho \exp(x_{10})/\beta_F]\}[1 + \gamma_1 + \rho \exp(x_{10})/\beta_F] \\ & + \epsilon[a_3 - a_1\rho \exp(x_{10})] > 0. \end{aligned} \quad (37)$$

Since a_1 , a_3 , γ_1 , β_F , and ρ are positive parameters, the constraint described by Eq. (36) is always satisfied. Similarly, Eq. (36) is equal to $\text{div}F > 0$, signaling the dissipative character of the system. This means that trajectories initiated from different conditions are attracted to a subspace of the state space. In addition, it is easy to verify that Eq. (35) has a pair of purely imaginary eigenvalues $Z_{1,2} = \pm i\Omega_H$ and the negative real root

$$Z_3 = -\left[a_3 + a_1 \left(\gamma_1 + \frac{\rho \exp(x_{10})}{\beta_F} \right) \right], \quad (38)$$

with

$$\Omega_H^2 = a_3 a_1 \left[1 + \epsilon + \gamma_1 + \frac{\rho \exp(x_{10})}{\beta_F} \right], \quad (39)$$

provided that

$$\begin{aligned} & \left[a_3 + a_1 \gamma_1 + \frac{a_1 \rho \exp(x_{10})}{\beta_F} \right] \left[1 + \epsilon + \gamma_1 + \frac{\rho \exp(x_{10})}{\beta_F} \right] \\ & - \epsilon a_1 \left[\gamma_1 + \frac{\rho \exp(x_{10})}{\beta_F} \right] = 0. \end{aligned} \quad (40)$$

This constraint (40) is important while calculating the critical values of the control parameters a_1 , a_3 , γ_1 , ρ , and ϵ , for a Hopf bifurcation of the equilibrium state X_0 . The period of this bifurcating periodic solution at X_0 is $2\pi/\Omega_H$. In general, Eq. (35) may be solved for all values of its coefficients. Figure 4 shows the plot of the roots in the complex plane where the common-base current gain α_F and the dimensionless parameter ρ vary in the intervals $]0,1[$ and $[0.01, 4 \times 10^5]$, respectively, with the parameters $\epsilon = 3.33333$, $a_1 = 0.0600$, $a_3 = 3.8431$, and $\gamma_1 = 2.1522$. This picture indicates that for certain values of the system's parameters, Hopf bifurcation and periodic solutions of the system may exist.

2. Existence of a limit cycle

It is well known that the key character of any stable oscillator is the existence of a limit cycle. In this section we show that steady state oscillation of the set of differential equation (25) maps onto an ellipselike closed trajectory space. For this purpose, from Eq. (25) it is straightforward to show

$$\begin{aligned} p_1 = & \frac{\beta_F}{4a_1 a_3 \rho (a_1 a_3 - 1)} \left\{ a_1^2 a_3 (1 + \beta_F)^2 - 4a_1^2 a_3^2 [\epsilon(1 - \beta_F) + 2 + 3\gamma_1] \right. \\ & \left. + a_1 [-2\epsilon(1 + \beta_F) + 4\epsilon a_3 (\beta_F - 1) + 4a_3 (a_3^2 - 2 - 2\gamma_1)] \right\}, \end{aligned} \quad (46)$$

$$\begin{aligned} p_2 = & \frac{\beta_F}{4a_3 \rho^2 (a_1 a_3 - 1)} \left\{ \beta_F a_1^2 a_3 \epsilon^2 (1 + \beta_F)^2 + 4a_1 a_3 (a_3^2 + \epsilon) (1 + \epsilon + \gamma_1) \right. \\ & \left. + a_1 \beta_F^3 \epsilon^2 [-1 + a_1 a_3 (1 + \gamma_1)] + a_1 a_3 \epsilon \rho g_0 [4 - \epsilon a_1 a_3 (1 + \beta_F^2)] + \epsilon a_3 - \epsilon a_1 \beta_F^2 (1 + 3\epsilon) + 2a_3 a_1^2 \epsilon (1 + \gamma_1) \right\}, \end{aligned} \quad (47)$$

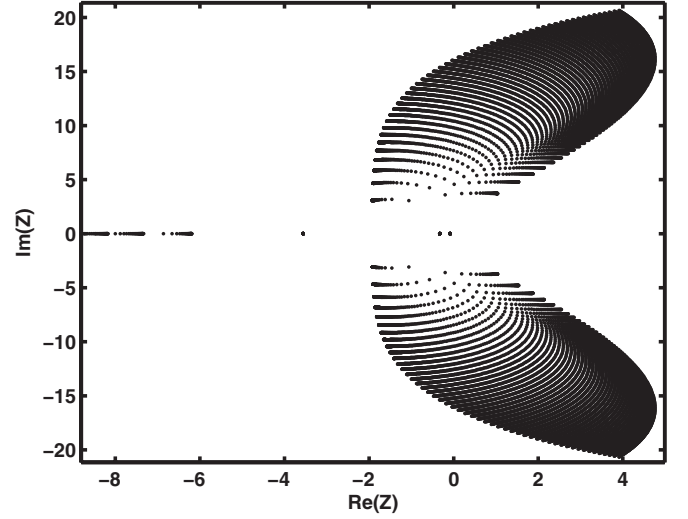


FIG. 4. Representation in the complex plane of the eigenvalues of the Jacobian matrix solutions of Eq. (35). The parameters of the system are $\epsilon = 3.33333$, $a_1 = 0.0600$, $a_3 = 3.8431$, $\gamma_1 = 2.1522$. The parameter β is used as a control parameter of the system and varies between 0.01 and 800; accordingly, $\phi(x_{10})$ varies between 0.01 and 4×10^5 .

that the temporal variation of x_2 and x_3 depends solely on x_1 . In fact,

$$\dot{x}_2 = -\epsilon [\dot{x}_1 + a_1 \gamma_1 x_1 + \rho a_1 f(x_1)/\alpha_F] \quad (41)$$

and

$$x_3 = -\dot{x}_1/a_1 - \gamma_1 x_1 - \rho f(x_1)/\beta_F, \quad (42)$$

while the dynamics of x_1 verifies the following nonlinear third-order differential equation:

$$\begin{aligned} \ddot{x}_1 + & \left[a_1 \gamma_1 + a_3 + \frac{a_1 \rho}{\beta_F} \exp(x_1) \right] \dot{x}_1 \\ & + a_1 a_3 \left[1 + \epsilon + \gamma_1 + \left(1 + \frac{a_1 \dot{x}_1}{a_3} \right) \frac{\rho}{\beta_F} \exp(x_1) \right] x_1 \\ & + \epsilon a_1^2 a_3 \gamma_1 x_1 + \frac{\epsilon a_1^2 a_3 \rho}{\alpha_F} [\exp(x_1) - g_0] = 0. \end{aligned} \quad (43)$$

This equation admits a periodic solution of the form (see the Appendix)

$$x_1(\tau) = A_0 + A_1 \sin(\Omega_{\text{osc}} \tau + \phi_0), \quad (44)$$

where the dc component A_0 satisfies the following equation:

$$\begin{aligned} & \exp(3A_0) + p_1 \exp(2A_0) + (p_2 + A_0 q_2) \exp(A_0) \\ & + p_3 + A_0 q_3 = 0, \end{aligned} \quad (45)$$

with

$$\begin{aligned}
p_3 = & \frac{\beta_F^2}{4a_1a_3\rho^2(a_1a_3 - 1)} (a_3\beta_F^2\epsilon^2(2 - a_3\rho g_0a_1^2)^2 - \rho a_3^2g_0(1 + \beta_F)^2 - 4\epsilon a_1a_3\gamma_1\beta_F(1 + \gamma_1) \\
& - a_3\epsilon^2 \{ \rho g_0a_1(\beta_F + 1)(\beta_F - 2) + \rho a_3a_1^2g_0[(1 + \beta_F)(1 + \gamma_1) + \beta_F^2\gamma_1] \\
& + 2\beta_F(-1 + 2a_3 - 2a_1a_3^2) \} + 8a_1\beta_F(1 + \gamma_1)\epsilon a_3^3 + 4a_1\beta_F a_3^3(1 + \gamma_1)^3 + a_3^2 \{ -4\beta_F \\
& + \epsilon[4(1 + \gamma_1)(-2 + \beta_F a_1^2\gamma_1) + \rho g_0(1 + \beta_F)] + 4\gamma_1\beta_F[a_1^2 + (2 + \gamma_1)(-1 + a_1^2\gamma_1)] \} \\
& + 2\epsilon\beta_F(1 + \beta_F)(1 + \gamma_1)(a_3 + a_1\gamma_1) - 4a_1a_3\beta_F\gamma_1(1 + \gamma_1)^2 + 2\rho g_0(1\beta_F)(a_1 + 2\gamma_1) \}, \quad (48)
\end{aligned}$$

$$q_2 = \frac{\epsilon\beta_F^2\gamma_1[-4 + a_1a_3\epsilon(1 + \beta_F)]}{4\rho^2(a_1a_3 - 1)}, \quad (49)$$

$$q_3 = \frac{\beta_F^2}{4a_1(a_1a_3 - 1)} \{ (1 + \beta_F)[1 + a_1a_3(1 + \epsilon + \gamma_1)] - a_3 - 4a_1\gamma_1 - 3a_1(1 + \epsilon) \}. \quad (50)$$

Similarly, the amplitude of the signal A_1 and the angular frequency Ω_{osc} are given as follows:

$$A_1^2 = \frac{4\epsilon\beta_F}{\rho \exp(A_0)} \left\{ \frac{\rho(\beta_F + 1)[\exp(A_0) - g_0a_3] + \beta_F a_3\gamma_1 A_0}{2a_3(1 - a_1a_3)[\beta_F(1 + \epsilon + \gamma_1) + \rho \exp(A_0)] - \epsilon\beta_F(1 + \beta_F)} \right\} \quad (51)$$

and

$$\Omega_{\text{osc}} = \Omega_H \left[1 + \frac{\rho a_1 a_3 A_1^2}{8\beta_F \Omega_H^2} \exp(A_0) \right]^{1/2}, \quad (52)$$

from which it appears that for small-amplitude signals, $A_1 \ll 1$, the frequency Ω_{osc} reduces to the Hopf frequency Ω_H . It is obvious that the periodic solution (44) strongly depends on the characteristic parameters of the MCO, namely, the common-base current gain of the transistor α_F . This behavior is sketched in Fig. 5 for $\gamma_1 = 2.1522$, $g_0 = 1.9294 \times 10^{-14}$, and $\rho = 571.7216$, where it appears that the dc component A_0 is almost constant for $\alpha_F < 0.6$. Similarly, the amplitude of the first harmonic linearly increases in this range of the parameter α_F . It appears also that the frequency of the signal decreases for increasing values of α_F or amplitude A_1 . Let us mention that the above analytical investigation is valid only if the amplitude A_1 is small compared to 1. This condition is satisfied for small values of the parameter α_F , or more precisely, for $\alpha_F < 0.4$ (see Fig. 5). The numerical simulations performed on Eq. (25), for different initial conditions close to the closed orbit of the above solution, end up on the same trajectory, indicating that this oscillation corresponds to a limit cycle.

C. Train of dark-compacton-like signal voltages

From the above investigations, it appears that under the condition $A_1 \ll 1$ (that is, $\alpha_F < 0.4$), oscillations of the MCO produce signal voltages of different types according to the output considered. Thus, at the gate S_3 , it appears that

$$V_{S_3}(\tau) = V_{03} \{ 1 - M \cos(\Omega_{\text{osc}}\tau + \phi_0) \Theta[\cos(\Omega_{\text{osc}}\tau + \phi_0)] \}, \quad (53)$$

since $V_{S_3} = V_T x_{S_3}$ and where $\Theta(U)$ is the step function,

$$\Theta(U) = \begin{cases} 0 & \text{if } U \leq 0, \\ 1 & \text{otherwise,} \end{cases} \quad (54)$$

with $V_{03} = E_2$ and $M = G\Gamma V_T A_1 \Omega_{\text{osc}} E_1 / E_2$. If the dc potentials E_1 and E_2 are chosen so that $M = 1$, the gate S_3 delivers a signal voltage with a shape close to that of the modulated compact dark solitary wave.

The above behavior of the MCO is a first step toward the generation of modulated dark-compacton-like signal voltages by the whole circuit. In fact, the dynamics of the MCO part is coupled to the NLTL through the equation

$$V_0(t) = \Gamma V_{S_3} V_S(t) + V_b, \quad (55)$$

where V_b is the bias voltage and V_0 the voltage at cell $n = 0$. This coupling can be interpreted as follows: The nonlinear transmission line described in Sec. II is supplied by the signal delivered at the output S_3 of the MCO and modulated by means of the summer as indicated in Fig. 1, so that the signal voltage at cell number 0 is given by Eq. (55). When the MCO part exhibits a stable limit cycle, this signal can be explicitly written as

$$V_0(t) = V_m \{ 1 - M \cos(\omega_p t + \phi_0) \Theta[\cos(\omega_p t + \phi_0)] \} \cos(\omega t) + V_b, \quad (56)$$

where $V_m = E_2$, and ω is the carrier frequency, which is a free parameter, but has to be chosen in the allowed frequency range of the NLTL, which behaves as a bandpass filter. To maintain the synchronization between the MCO and the NLTL, the parameter ω_p which is related to the fundamental frequency of the MCO by $\omega_p = \Omega_{\text{osc}} \omega_{\text{ref}}$ has to match the temporal pulse width in the NLTL. In fact, in the absence of loss (undamped NLTL), the temporal dark compacton width τ_s and the compacton repetition rate f are given by

$$\tau_s = \frac{\pi}{\mu_c v_c} \quad \text{and} \quad f = v_c / \ell, \quad (57)$$

where μ_c and v_c are the width parameter and the compacton speed along the transmission line, respectively, while ℓ is the spacing between two adjacent compactons. Since ℓ

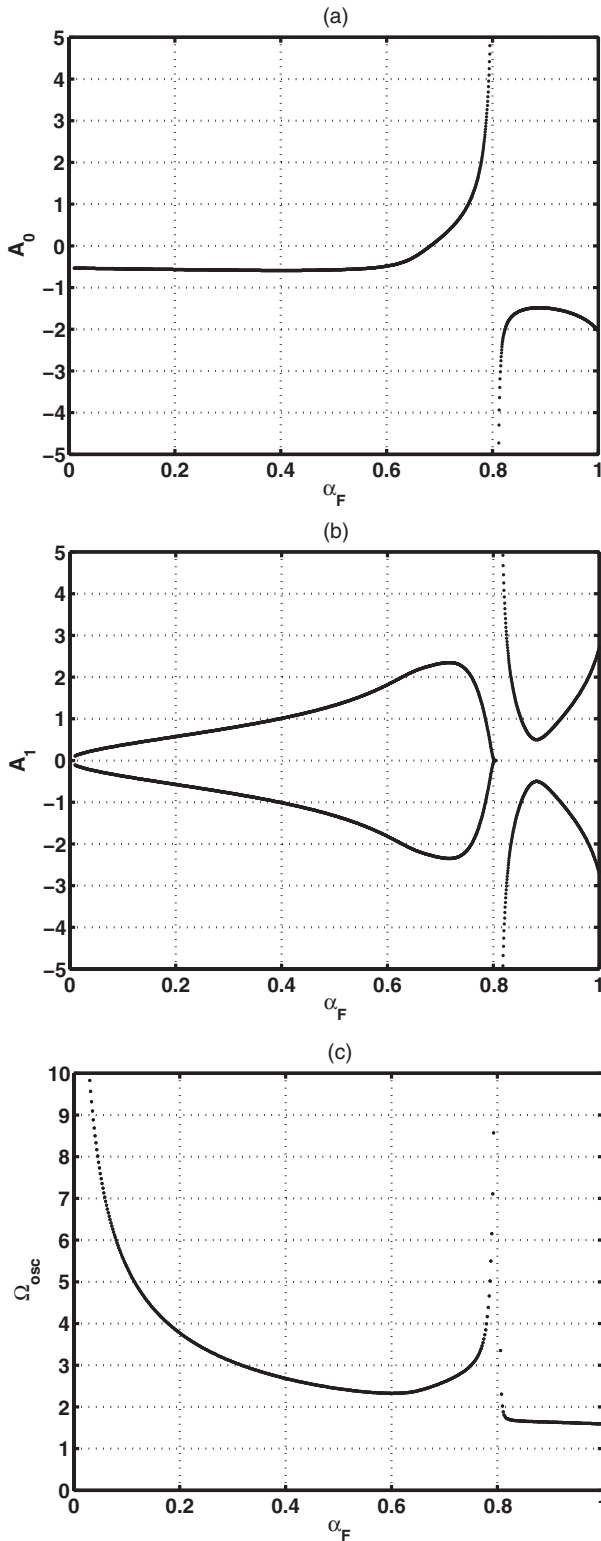


FIG. 5. Variation of the parameters of the harmonic solution (44) of the system as functions of α_F and with $f_0 = 1.9294 \times 10^{-14}$ and $\rho = 571.7216$.

corresponds to the distance traveled by the compact signal during one period of the signal $S_3(t)$, it follows that $\ell = v_c/f_p$. Similarly, because the temporal pulse width is half the period of the compact signal, that is, $\tau_s = 1/2f_p$, it appears that the mathematical conditions for synchronized dynamics between

TABLE I. Set of parameters of the modified Colpitts oscillator. The BJT transistor Q2N2222 BJT is the Quad two common NPN bipolar junction transistor.

Circuit components	Circuit elements	Numerical values
Q2N2222 BJT	V_{th}	25 mV
	T	295 K
	R_B	10 Ω
	β	255.9
	I_s	14.34×10^{-15} A
Voltage polarization	V_{cc0}	12 V
	V_{cc1}	6 V
	V_{DD}	12 V
	E_1	5 V
	E_2	0.25 V
	$v_b \equiv E_4$	1.5 V
AD633 multiplier	Γ	0.1 V ⁻¹
Resistors	R_1	400 Ω
	R_2	20 Ω
	R_3	300 Ω
	R_4	2000 Ω
	χ	0.35
Inductance	L_1	0.2 mH
Capacitance	C_1	0.32 nF
	C_2	0.096 nF
BA220 diode	V_{th}	0.5 V
	G	0.8

the MCO and the NLTL parts are

$$\mu_c v_c / 2\pi \approx f_p \quad \text{and} \quad f = f_p = \frac{\Omega_{osc}}{2\pi} \frac{1}{\sqrt{L_1 \frac{C_1 C_2}{C_1 + C_2}}}, \quad (58)$$

where $f_p = \omega_p / 2\pi$. This equation associated with the analytical expression of v_c is very important in the design guidelines of the generator.

IV. NUMERICAL SIMULATIONS

In this section, we first set the numerical values used for the circuit elements as well as for the parameters characterizing the electronic components. Next, details of the numerical integrations performed on the mathematical equations describing the dynamics of the MCO part are given, and finally the results of the PSPICE simulations of the oscillator's circuit. In fact, the parameters used in the analysis are listed in Table I for the MCO part while the characteristic parameters of the NLTL are $V_d = 1.5$ V for the polarization voltage, and $L_s = 0.47$ mH and $L_p = 0.22$ mH for the inductances. The nonlinear capacitor in the series branch is an X_D2D1 diode or a Pspice BB112 diode with $C_{0s} = 10$ pF and series resistance $R_s = 0.2$ Ω , while the nonlinear capacitor in the shunt branch D_1N5225 diode, a N silicon metal-oxide-semiconductor varactor diode, with $C_{0p} = 316$ pF and associated resistance $R_p = 0.2$ Ω . The resistor R_5 is used as a control parameter of the system and its value may vary according to the desired phenomena. In fact, analytical results indicate a threshold in R_5 under which the oscillations of the MCO are established. Similarly, since R_{EE} and ρ are R_5 dependent, they are not listed in the table, while

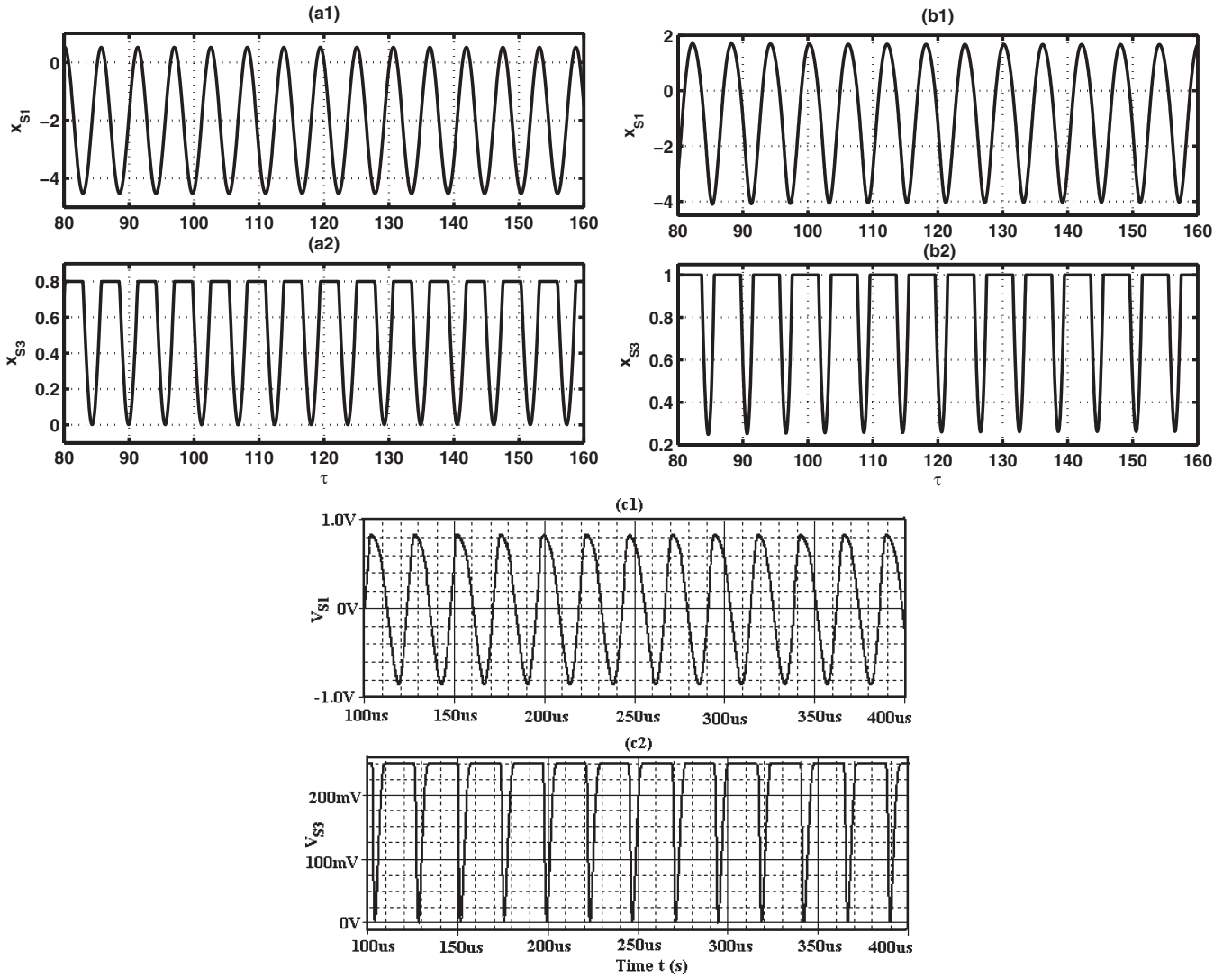


FIG. 6. Behavior of the MCO at gates S_1 (top panels) and S_3 (bottom panels): (a) Analytical result, (b) result of the numerical integration, and (c) PSPICE simulations. The parameters of the system are defined by Eq. (59) with the control parameter $R_5 = 60 \Omega$.

the summer and multiplier are chosen in the PSPICE netlist. With the above characteristics of the circuit, the following value of the fundamental angular frequency of the MCO is obtained: $\omega_{\text{ref}} = 8.23 \times 10^6 \text{ rad/s}$ leading to $f^* = 1.31 \text{ MHz}$.

To check the above analytical results performed on the MCO, the set of equations (25) governing the dynamics of the MCO in dimensionless units is first solved numerically by means of the fourth-order Runge-Kutta scheme with the time step $\Delta\tau = 2 \times 10^{-3}$. The parameters of this equation are calculated according to the numerical values of the electronic components listed in Table I. It follows that

$$\epsilon = 3.333, \quad a_1 = 0.6005, \quad a_3 = 0.3843. \quad (59)$$

In addition, taking for example the value of the control parameter as $R_5 = 60 \Omega$, we get the following numerical values of the R_5 -dependent parameters: $R_{EE} = 41 \Omega$, $g_0 = 5.99 \times 10^{-13}$, $\rho = 18.4021$, and $\gamma_1 = 0.4855$. The results of these numerical simulations displayed in Fig. 6 show a signal at gate S_3 with a compact shape obtained from harmonic oscillations of the Colpitts oscillator at gate S_1 , as shown in the phase-plane plot $(x_1, x_1 + x_2)$ (see Fig. 7). However, at

large values of R_5 , for example, $R_5 = 250 \Omega$, the signal at the output S_1 still remains coherent but contains more than one harmonic, and consequently the gate S_3 no longer delivers a harmonic signal, as illustrated in Fig. 8. This means that the parameters of the circuit in general and the numerical value of R_5 in particular have to be selected carefully so that the signal delivered at the output S_1 has a sinusoidal shape. The numerical experiments indicate that R_5 may vary in the ranges $[0.5 \Omega, 4.2 \Omega]$ and $[55 \Omega, 200 \Omega]$ without noticeable change of the sinusoidal shape delivered by S_1 . In addition, the pulse width and signal frequency are less affected by this variation of the control parameter. Similarly, the fact that the use of different initial conditions to run the integration of the circuit's equations (25) leads to the same closed orbit in the phase plane indicates the presence of a stable limit cycle.

Next, the set of equations (25) and (7) is also integrated numerically with the coupling (55) in order to check the validity of the analytical condition of synchronization of the two subsystems. The parameters of the circuits are carefully chosen so that the temporal width τ_s matches the temporal width of the compact dark solitons exhibited by the NLTL

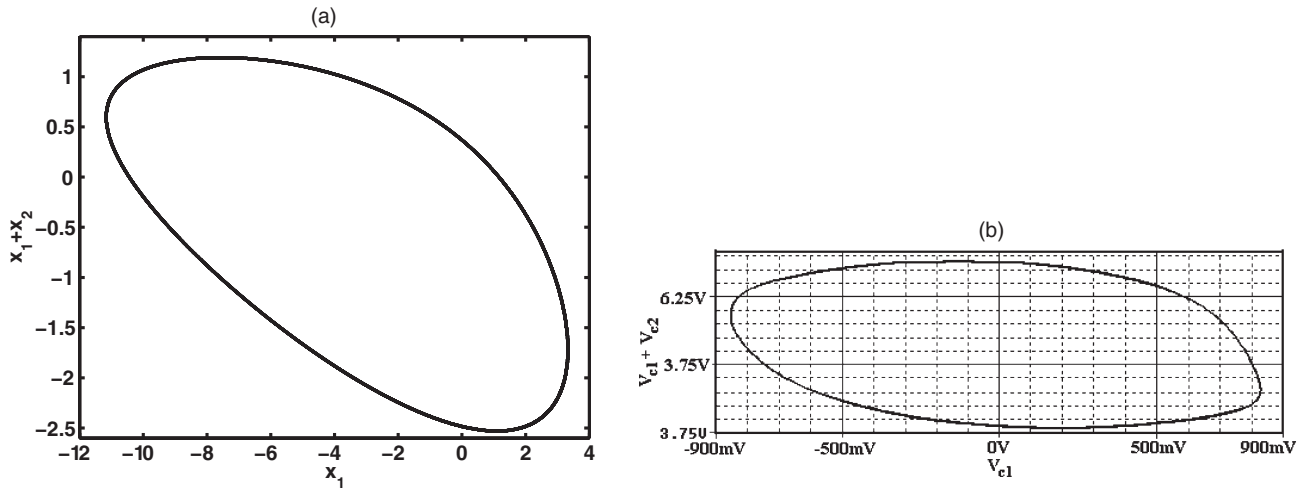


FIG. 7. Typical phase space obtained with the parameters of the system identical to those of Fig. 6: (a) Analytical, (b) numerical, and (c) PSPICE results.

and described by Eqs. (20) and (57). The numerical results are in good agreement with the analytical predictions and simulations of the circuit diagram. Figure 9 shows the compact modulated signal voltages at cells 100 and 130 of the NLTL, respectively, obtained through the PSPICE software. It appears that the signal’s amplitude decays in propagation due to losses of the network components such as the nonlinear diodes and the linear inductors. Examples of the circuit’s

characteristics as well as the resulting circuit performance are $v_c = 0.91$ cells/ μs , $\tau_s = 5.87 \mu s$, and $f = 0.437$ MHz for the pulse’s speed, width, and repetition rate, respectively, at the working frequency 0.87 MHz belonging to the allowed frequency band [0.86,0.96] (MHz) of the circuit.

The performance strongly depends on the carrier frequency (working frequency) due to the dependence of the circuit’s characteristics on this input parameter. The performance may

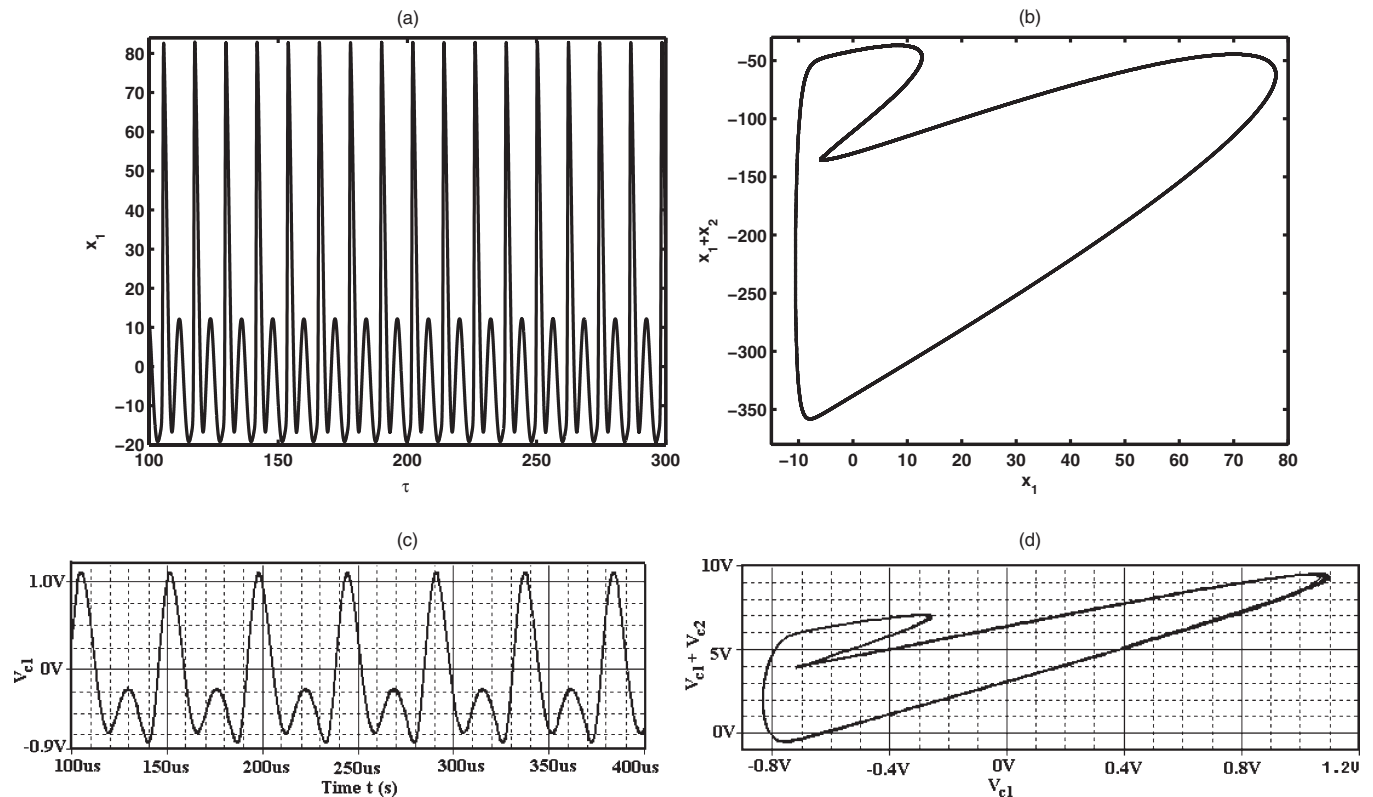


FIG. 8. Behavior of the MCO at the gate S_1 : (a) signal $x_1(t)$ and (b) phase portrait, resulting from the numerical integrations; (c) signal voltage $V_1(t)$ and (d) corresponding phase portrait, from the PSPICE simulations. The parameters of the system are still given by Eq. (59) but the control parameter is $R_5 = 250 \Omega$. It appears that the behavior of the MCO is no longer harmonic.

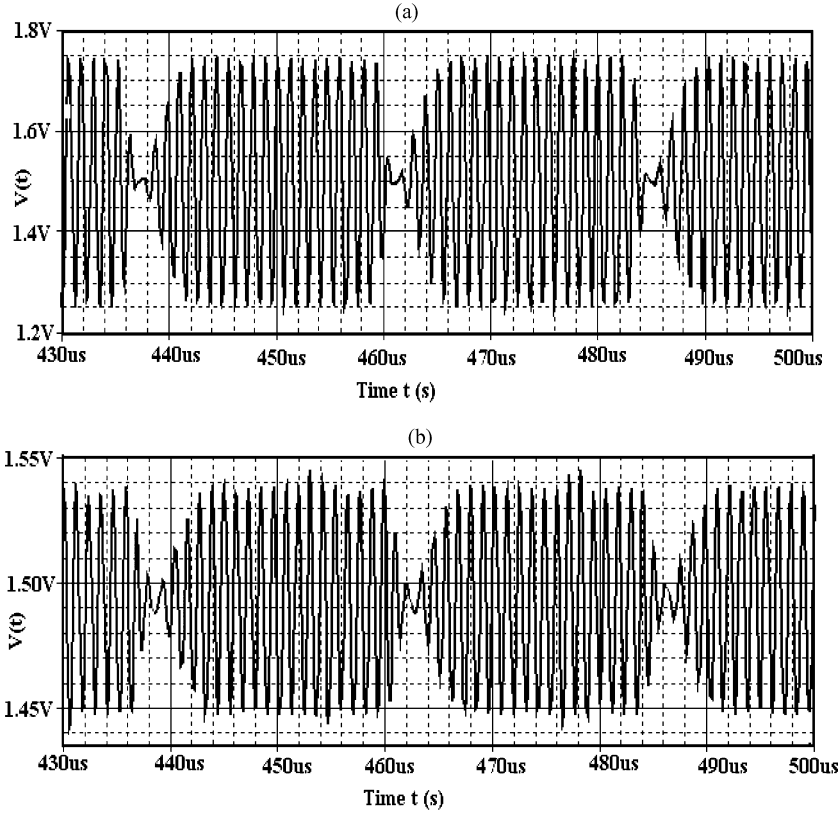


FIG. 9. Results of the simulation of the NLTL dark compacton generator (MCO + NLTL part) by means of the PSPICE professional simulator. Signals at two different cells of the NLTL: (a) cell 100 and (b) cell 130. The amplitude of the signal at cell 130 is smaller than that at cell 100 due to the dissipation effects induced by the losses of the NLTL. The parameters of the circuit are given in Sec. IV and Table I.

be improved by an appropriate choice of the values of the inductance and capacitances L_1 , C_1 , and C_2 for the MCO and L_p , L_s , C_{0s} , and C_{0p} for the NLTL. For example, taking the inductance on the order of nanohenries and the capacitance on the order of femtofarads, the circuit performance is considerably improved.

V. CONCLUSIONS

In this paper, we have proposed an electrical device working as a generator of a train of modulated dark-compacton-like signals. The device consists of a modified Colpitts oscillator associated with a NLTL. The NLTL part is a nonlinear electrical transmission line with intersite nonlinearities allowing the propagation of modulated dark compacton signals with interesting properties compared to those of solitons. First, after deriving the equations of state governing the dynamics of the MCO part, we showed that, in certain regimes of the control parameter, the system may exhibit a limit cycle characterizing the presence of oscillation, where the amplitude can be modified by varying the dc potential E_2 . Through the Van der Pol method, the frequency of oscillations of the system was then evaluated. Next, the performance of the generator, namely, the pulse width and the repetition rate, was also derived; it is closely connected to the fundamental frequency of the MCO. Accordingly, the performance of the device can be controlled from the MCO components while the amplitude of the signal is controlled by varying the dc potential E_2 . However, the characteristics of the NLTL components must be chosen carefully in order to avoid mismatch between the temporal width of the dark compactons and the pulse width generated by the MCO. Finally, the simulation of the circuit through the PSPICE professional simulator has demonstrated

its capacity to work as a 0.4 MHz generator of a train of modulated compact dark signals with temporal width $5.87 \mu\text{s}$. This performance is not dictated by the design criteria or technical characteristics of the device but only by our difficulty to use the appropriate components of the NLTL in the PSPICE netlist. Thus, with the appropriate components it is possible to obtain for this generator performance characteristics up to gigahertz for the repetition rate and nanoseconds for the pulse temporal width.

APPENDIX: DERIVATION OF A HARMONIC SOLUTION FOR THE MCO

In order to solve Eq. (43), let us use Van der Pol methods [26,27]. So the solution of the above equation is found as

$$x_1(\tau) = A_0(\tau) + A_1(\tau) \sin[\psi(\tau)], \quad (\text{A1})$$

with $\psi(\tau) = \Omega_{\text{osc}}\tau + \phi(\tau)$. Taking into account the fact that $A_0(\tau)$, $A_1(\tau)$, and $\phi(\tau)$ do not vary considerably in one period interval, the first, second, and third derivatives of $x_1(\tau)$ with respect to time can be calculated as

$$\begin{aligned} \dot{x}_1 &= \Omega_{\text{osc}} A_1 \cos \psi, & \ddot{x}_1 &= -\Omega_{\text{osc}}^2 A_1 \sin \psi, \\ \ddot{x}_1 &= -\Omega_{\text{osc}}^3 A_1 \cos \psi + \Omega_{\text{osc}}^2 \dot{A}_0, \end{aligned} \quad (\text{A2})$$

with the constraints

$$\begin{aligned} \dot{A}_0 + \dot{A}_1 \sin \psi + A_1 \dot{\phi} \cos \psi &= 0, \\ \dot{A}_1 \cos \psi - A_1 \dot{\phi} \sin \psi &= 0. \end{aligned} \quad (\text{A3})$$

By inserting the set of equations (A2) into Eq. (43), one obtains the following expression for \dot{A}_0 :

$$\begin{aligned} \dot{A}_0 = h_1(A_0, A_1, \psi) = & A_1 \cos \psi + A_1 \sin \psi \left[a_3 + a_1 \gamma_1 + \frac{a_1 \rho \exp(A_0 + A_1 \sin \psi)}{\beta_F} \right] \\ & - \frac{a_1 a_3 A_1}{\Omega_{\text{osc}}^2} \left[(1 + \epsilon + \gamma_1) \cos \psi + (\cos \psi + a_1 A_1 \cos^2 \psi) \frac{\rho}{\beta_F} \exp(A_0 + A_1 \sin \psi) \right] \\ & - \epsilon a_1^2 a_3 \gamma_1 (A_0 + A_1 \sin \psi) + \frac{\epsilon a_1^2 a_3 \rho}{\alpha_F} [g_0 - \exp(A_0 + A_1 \sin \psi)], \end{aligned} \quad (\text{A4})$$

while from the set of equations (A3), we have

$$\dot{A}_1 = -\sin(\psi)h_1, \quad A_1 \dot{\phi}_0 = -\cos(\psi)h_1. \quad (\text{A5})$$

Taking the average of the set of \dot{A}_0 , \dot{A}_1 , and $A_1 \dot{\phi}_0$ in the time interval corresponding to $\psi \in [0, 2\pi]$, i.e.,

$$\begin{aligned} \dot{A}_0 &= \frac{1}{2\pi} \int_0^{2\pi} h_1(A_0, A_1, \psi) d\psi, \quad \dot{A}_1 = \frac{1}{2\pi} \int_0^{2\pi} -\sin(\psi)h_1(A_0, A_1, \psi) d\psi, \\ A_1 \dot{\phi}_0 &= \frac{1}{2\pi} \int_0^{2\pi} -\cos(\psi)h_1(A_0, A_1, \psi) d\psi, \end{aligned} \quad (\text{A6})$$

the set of equations (A4) and (A5) leads to the following set of ordinary differential equations:

$$\begin{aligned} \dot{A}_0 &= \frac{\epsilon a_1^2 a_3}{\Omega_{\text{osc}}^2} \left(\frac{g_0 \rho}{\alpha_F} - \gamma_1 A_0 \right) + \frac{\rho a_1 \exp(A_0)}{2\beta_F} \left[(1 - a_1 a_3) A_1^2 - \frac{\epsilon a_1 (1 + \beta_F)(4 + A_1^2)}{2\Omega_{\text{osc}}^2} \right], \\ \dot{A}_1 &= \frac{A_1}{2} \left(\frac{\epsilon a_3 a_1^2 \gamma_1}{\Omega_{\text{osc}}^2} - a_3 - a_1 \gamma_1 \right) - \frac{\rho a_1 A_1 \exp(A_0)}{2\beta_F} \left[1 + \frac{3A_1^2}{8} - \frac{a_1 a_3 A_1^2}{4} - \frac{a_1 a_3 \epsilon (1 + \beta_F)(8 + A_1^2)}{8\Omega_{\text{osc}}^2} \right], \\ A_1 \dot{\phi} &= \frac{A_1}{2\Omega_{\text{osc}}} \left[-\Omega_{\text{osc}}^2 + a_1 a_3 (1 + \epsilon + \gamma_1) + \frac{a_1 a_3 (8 + A_1^2) \rho \exp(A_0)}{8\beta_F} \right]. \end{aligned} \quad (\text{A7})$$

The solution of the set of equations (A7) is stationary if $\dot{A}_0 = \dot{A}_1 = A_1 \dot{\phi} = 0$, leading to

$$\Omega_{\text{osc}}^2 = a_1 a_3 \left[1 + \epsilon + \gamma_1 + \left(1 + \frac{A_1^2}{8} \right) \frac{\rho}{\beta_F} \exp(A_0) \right], \quad (\text{A8})$$

$$A_1^2 = \frac{4\epsilon\beta_F}{\rho \exp(A_0)} \left\{ \frac{\rho(\beta_F + 1)(\exp(A_0) - g_0 a_3) + \beta_F a_3 \gamma_1 A_0}{2a_3(1 - a_1 a_3) [\beta_F(1 + \epsilon + \gamma_1) + \rho \exp(A_0)] - \epsilon\beta_F(1 + \beta_F)} \right\}, \quad (\text{A9})$$

where A_0 verifies Eq. (45). The solution of Eq. (43) is then given by

$$x_1(\tau) = A_0 + A_1 \sin(\Omega_{\text{osc}} \tau + \phi_0). \quad (\text{A10})$$

-
- [1] R. Hirota and K. Suzuki, *J. Phys. Soc. Jpn.* **28**, 1366 (1970).
[2] M. Remoissenet, *Waves Called Solitons*, 3rd ed. (Springer-Verlag, Berlin, 1999).
[3] Y. S. Kivshar and B. Luther-Dvies, *Phys. Rep.* **298**, 81 (1998).
[4] H. A. Haus and W. S. Wong, *Rev. Mod. Phys.* **68**, 423 (1996).
[5] E. Afshari, H. S. Bhat, A. Hajimiri, and J. E. Marsden, *J. Appl. Phys.* **99**, 054901 (2006).
[6] K. Narahara and M. Nakamura, *Jpn. J. Appl. Phys.* **42**, 6327 (2003).
[7] H. K. Nguena, S. Noubissi, and P. Woaf0, *J. Phys. Soc. Jpn.* **73**, 1147 (2004).
[8] M. Nguimdo, S. Noubissie, and P. Woaf0, *J. Phys. Soc. Jpn.* **77**, 124006 (2008).
[9] K. Narahara, *Jpn. J. Appl. Phys.* **42**, 5508 (2003).
[10] M. Kahrs, *IEEE Trans. Microwave Theory Tech.* **51**, 1787 (2003).
[11] R. Y. Yu, M. Reddy, J. Pusl, S. T. Allen, M. Case, and M. J. W. Rodwell, *IEEE Trans. Microwave Theory Tech.* **43**, 721 (1995).
[12] G. F. Ross, US Patent No. 3,728,632 (17 April 1973).
[13] D. S. Ricketts, X. Li, N. Sun, K. Woo, and D. Ham, *IEEE J. Solid-State Circuits* **42**, 1657 (2007).
[14] D. Yemélé and F. Kenmogné, *Phys. Lett. A* **373**, 3801 (2009).
[15] P. Rosenau and J. M. Hyman, *Phys. Rev. Lett.* **70**, 564 (1993).
[16] W. J. Tomlinson, R. J. Hawkins, A. M. Weiner, J. P. Heritage, and R. N. Thurston, *J. Opt. Soc. Am. B* **6**, 329 (1989).
[17] F. Daschelt and W. Schwartz, *IEEE Trans. Circ. Syst. I* **48**, 1498 (2001).

- [18] M. Wada, J. Kawata, Y. Nishio, and A. Ushida, *IEICE Trans. Fundamentals of Electronics, Communications and Computer Sciences* **E83-A**, 563 (2000).
- [19] N. F. Rulnikov, M. M. Sushchik, L. S. Tsimring, and A. R. Volkovskii, *IEEE Trans. Circuits Syst. I* **48**, 1436 (2001).
- [20] G. Heidari-Bateni and C. D. McGillen, *IEEE Trans. Commun.* **42**, 1524 (1994).
- [21] G. M. Maggio, M. di Bernardo, and M. Kennedy, *IEEE Trans. Circuits Syst.* **47**, 1160 (2000)
- [22] G. M. Maggio, O. de Feo, and M. P. Kennedy, *IEEE Trans. Circuits Syst.* **46**, 1118 (1999).
- [23] M. Kennedy, *IEEE Trans. Circuits Syst.* **41**, 771 (1994).
- [24] P. Marquié, J. M. Bilbault, and M. Remoissenet, *Phys. Rev. E* **49**, 828 (1994); **51**, 6127 (1995).
- [25] R. M. Corless, G. H. Gonnet, D. E. G. Hare, D. J. Jeffrey, and D. E. Knuth, *Adv. Comput. Math.* **5**, 329 (1996).
- [26] C. Hayashi, *Nonlinear Oscillations in Physical Systems* (McGraw-Hill, New York, 1964).
- [27] A. H. Nayfeh and D. T. Mook *Nonlinear Oscillations* (John Wiley and Sons, New York, 1979).